Development of a millimeter-long Travelling wave THz photomixer

Fuanki Bavedila, Charbel Tannoury, Quyang Lin, Sylvie Lepilliet, Vanessa Avramovic, Etienne Okada, Dmitri Yarekha, Marc Faucher, David Troadec, Jean-Francois Lampin, et al.

Development of a millimeter-long Travelling wave THz photomixer

F. Bavedila, C. Tannoury, Q. Lin, S. Lepilliet, V. Avramovic, E. Okada, D. Yarekha, M. Faucher, D. Troadec, J–F. Lampin, G. Ducournau, G. Loas, V. Magnin and E. Peytavit

[1]***Abstract*— THz sources based on the optical-heterodyne (photo)mixing in an ultrafast photodetector are very promising since they operate at room temperature, are potentially compact, cost-efficient and, above all, are widely frequency-tunable. However, their widespread use is currently hampered by available power levels in the µW range at THz frequencies. We present here a travelling wave structure, with millimeter level coherence length at THz frequencies opening the way to large active area (~4000 µm^2) photomixing devices capable of handling optical pump power beyond 1 W well beyond the capabilities of standard lumped-element devices using small active areas (<50 µm^2) needed to maintain a capacitance level (<10 fF) compatible with THz operation. It is based on a silicon nitride waveguide coupled to a membrane-supported low-temperature-grown GaAs photoconductor embedded in a coplanar waveguide. Milliwatt power levels up to 1 THz and still above 1 µW up to 4 THz are expected according to the optoelectronics model of this device elaborated in this study. Experimentally, the frequency response of a 1-mm-long structure, measured up to 100 GHz by using the beatnote produced by two 780-nm-DFB lasers, shows clearly the expected travelling wave signature consisting in a 6-dB-decrease ending at ~50 GHz when the contribution of the backward travelling wave is fully cancelled, following by a constant level up to ~100 GHz. The experimental demonstration of operation in the travelling wave regime is a first step towards the fulfillment of the original promises of this concept in terms of power level and frequency bandwidth.**

***Index Terms*— Photomixing, THz sources, Ultrafast photodetectors, Travelling Wave devices**

I. Introduction

One of the most promising monochromatic and widely tunable solid state THz sources operating at room temperature is based on the mixing of two laser frequencies in an ultrafast photodetector [1–4]. The spatial overlap of two slightly detuned optical laser beams produces a beatnote frequency located anywhere within the THz frequency band despite a negligible relative frequency sweep of the pump lasers. A photodetector, also called photomixer, illuminated by this two-frequencies laser beam, generates a THz photocurrent radiated in free space if coupled to a THz antenna. This technique is thus intrinsically wideband, limited by the photodetector electrical bandwidth, and is potentially compact when the optical pump power is provided by semiconductor laser diodes. THz photomixers are now key components of commercial THz spectroscopy systems [5,6] and have enabled the race to high data rate in THz wireless communications by bridging the gap between optical fiber and wireless communications technologies [7]. However, despite the great research effort made last years, these sources present power levels which are still in the µW range around 1 THz [8–13]. State of the art photomixers i.e. uni-travelling carrier photodiodes or photoconductors using sub-picosecond lifetime photoconductive materials, have indeed carrier-transport related bandwidth below 500 GHz resulting in a low efficiency at THz frequencies [14], [15]. In addition, THz operation requires sub-picosecond RC time constants and sub-10 fF electrical capacitances bringing with them restricted device sizes (<50 µm^2) leading to limited power dissipation capabilities (<~50 mW) and saturation photocurrents (~10 mA). The most direct way to achieve higher output THz powers is to increase their size beyond a level (>1000 µm^2) enabling watt level pump powers easily available by using commercial NIR laser and amplifiers at wavelengths in the range 780 nm -1550 nm. Travelling wave (TW) structures aimed at converting laser beams with time dependent intensities into RF or THz waves have been proposed theoretically many years ago as an alternative to lumped-element photodetectors to obtain large active area/volume devices while keeping large electrical bandwidths [16,17]. In this architecture, TW (photo)currents are induced in a metallic THz waveguide (rectangular waveguide [16] and coplanar waveguide [17]) thanks to a monolithically-integrated photoconductor illuminated by a light beam propagating in the same direction as the THz waves. The frequency response of a TW photomixer does not depend on its electrical capacitance but on the phase matching between the optical pump and the THz waves generated along the structure. Ever since this architecture was considered, numerous structures have been proposed to take advantage of their intrinsic large power capabilities to develop high power and high speed photodetectors for high data rate optical communications and naturally for the generation of THz waves [18–24]. As shown in Fig. 1, these devices were based on standard III-V semiconductor optical waveguides coupled to PIN or MSM photodetector structures whose metallic contact electrodes define also a microwave coplanar waveguide (CPW). This design leads to a large mismatch between the group index of the optical mode (n_g~3.3 in III-V semiconductors) and the phase index of the CPW fundamental propagation mode (n_g~2.7). Furthermore, doped layers (PIN) and reduced inter electrode spacing required for the embedded photoconductor lead to propagation losses

[1] This work was supported by the French Research Agency (Grant: ANR-15-CE24-0004), RENATECH (French Network of Major Technology Centres), Lille University, and the 'Région Hauts-de-France'. F. Bavedila, C. Tannoury, Q. Lin, S. Lepilliet, V. Avramovic, E. Okada, D. Yarekha, M. Faucher, D. Troadec, J–F. Lampin, G. Ducournau, V. Magnin and E. Peytavit are with Institute of Electronics, Microelectronics and Nanotechnology, UMR 8520 - IEMN, University of Lille, CNRS, Centrale Lille, Univ. Polytechnique Hauts-de-France, F-59000 Lille, France (e-mail: fuanki.bavedila@vmicro.fr, tannoury@iemn.fr, lin.etu@univ-lille.fr, lepilliet@iemn.fr, avramovic@iemn.fr, okada@iemn.fr, yarekha@iemn.fr, faucher@iemn.fr, troadec@iemn.fr, lampin@iemn.fr, ducournau@univ-lille.fr, magnin@univ-lille.fr, peytavit@univ-lille.fr). G. Loas is with Institut Foton, UMR 6082 / CNRS - Univ Rennes – INSA (e-mail: loas@univ-rennes1.fr)

often larger than 10 dB/mm beyond 100 GHz [23]. In addition, it is well known that CPW on bulk substrate suffer from radiation losses increasing as the frequency cubed avoiding any practical use of this waveguide for length >100 µm at frequency above 1 THz [25]. This explained mostly why the active length of these photodetectors, with the exception of that one studied in [19], equal to the optical absorption length is often lower than 50 µm. In the frequency range considered (< 500 GHz), these photoconductors are not really distributed and their limited size avoid any significant increase of their power dissipation and saturation photocurrent capabilities.

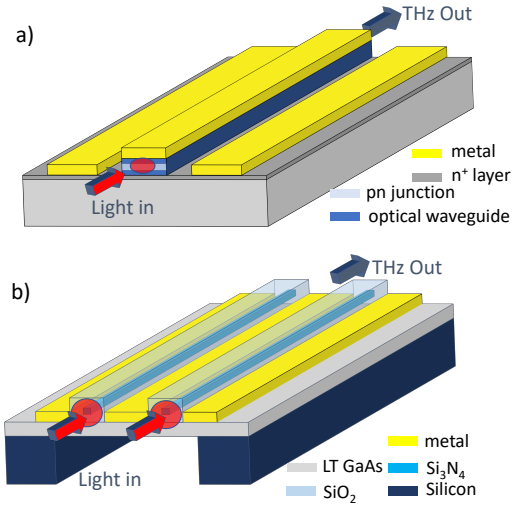

Fig. 1. Travelling wave photodetectors architectures: a) previous art and b) proposed structure.

In [19], the authors take advantage of the n-doped contact layer of the PIN junction to design a slow wave waveguide (n~3), mixed between a CPW and a microstrip waveguide. However, the thickness of the intrinsic semiconductor layer (1.2 µm) used in the PIN structure leads to a cut-off frequency related to the electron transit time not compatible with THz operation. A cut-off frequency below 5 GHz has been measured on a 1.25-mm-long device. Again, there is no convincing evidence of travelling wave operation here since the frequency response of this device has been characterized only up to 10 GHz. As a matter of fact, the only TW photodetectors showing very promising results as THz photomixers were based on vertical illumination and not on integrated optical waveguide. The phase-matching was then achieved by tuning the incidences angles of the two free space laser beams [26]. Elliptical spots were thus needed limiting the active length at a value of approximately 200 µm. In this work, we have designed, fabricated and characterized a new architecture of TW photomixer aimed at overcoming the limitations of the previous structures based on integrated optical guide, i.e., 1) the phase mismatch between the optical pump and the THz waves generated along the structure and 2) the propagation loss of the THz waveguide. It is based on a silicon nitride waveguide evanescently coupled to a membrane-supported low-temperature-grown GaAs ultrafast photoconductor, whose contact electrodes serve also as metallic strips of a THz coplanar waveguide (see Fig. 1b). We will present in the following parts, the design, fabrication and characterization of the device including its building blocks, i.e the optical waveguide based on a silicon nitride core and silicon oxide cladding deposited at low temperature (300 °C) and the LT-GaAs membrane-supported CPW.

II. TW PHOTOMIXER DESIGN PRINCIPLE

A. Principle

The THz waves produced along the photodetector due to the continuous absorption of the optical beating wave (beatnote angular frequency $\omega_b = 2\pi f_b$) interfere constructively if the phase velocity of the THz waves (v_φ^t) is equal to the group velocity of the optical wave (v_g^o). This phase matching condition resembles in principle to the one existing in the THz sources based on difference frequency generation in nonlinear crystals [27].

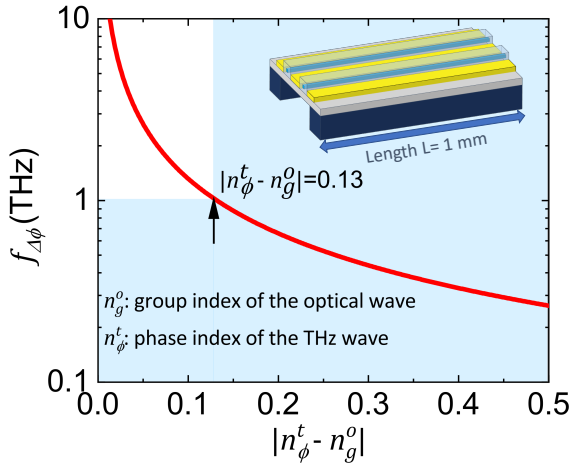

Fig. 2. Calculated cutoff frequency $f_{\Delta\phi}$ (defined as the frequency of 3dB loss in output power due to phase mismatch) as a function of the difference between the effective group index of the optical pump and the effective phase index of the THz waves, $\Delta n = |n_\varphi^t - n_g^o|$. Achieving $f_{\Delta\phi} > 1$ THz requires $\Delta n < 0.13$.

When perfect phase matching is not realized, it is shown in appendix A, by assuming a photocurrent generation constant along the device, that the output power (P_{THz}) available at the output of a TW photodetector of length L has a cardinal sinus dependency on the frequency:

$$P_{THz} \propto sinc^2\left[\frac{\omega_b}{2c}\left(n_\varphi^t - n_g^o\right)L\right] \quad (1)$$

where c is the vacuum velocity of light, n_φ^t is the effective phase index ($n_\varphi^t = c/v_\varphi^t$) of the THz wave and n_g^o ($n_g^o = c/v_g^o$) is the effective group index of the optical wave. From Eq. 1, for a given length L, it is possible to calculate a 3-dB-cutoff frequency related to the phase mismatch ($f_{\Delta\varphi}$) as a function of the effective index mismatch $\Delta n = |n_\varphi^t - n_g^o|$. It can be seen in Fig. 2 that for a millimeter-long active area, $\Delta n < 0.13$ is required to achieve $f_{\Delta\varphi} > 1$ THz. If we keep in mind that, in addition, the propagation loss of the THz waveguide must be limited, this simple model shows that the phase-matching requirement is hard to fulfill in the case of a THz photomixer with millimeter long active area. Furthermore, it becomes obvious that the previous attempts using standard CPW waveguide coupled to semiconductor optical waveguide had little chance of success. In the following, we will show that our design based on a silicon nitride waveguide evanescently coupled to a membrane-supported low-temperature-grown GaAs ultrafast photoconductor, initially proposed some years ago by one of the authors of this study [28], fulfills these requirements.

B. Membrane-supported coplanar waveguide photodetector

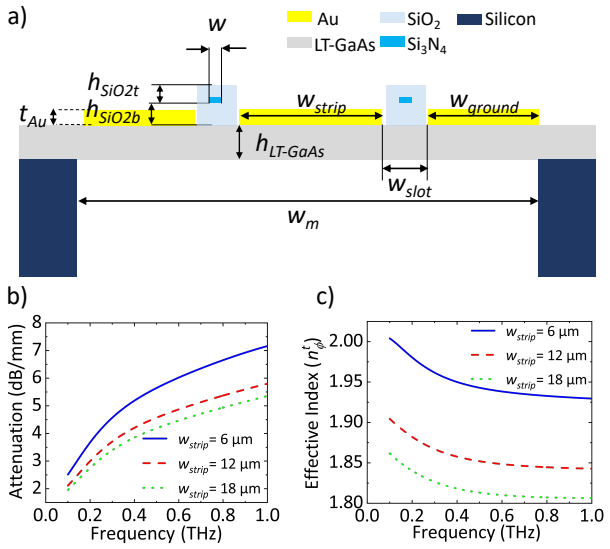

Fig. 3. a) Schematic of the proposed device b) THz propagation loss and c) effective index of the CPW odd-mode as a function of frequency with central strip width w_{strip} = 6, 12 and 18 µm, w_{ground} = 6 µm, w_m = + ∞, w_{slot} = 2 µm, $h_{LT\text{-}GaAs}$ = 700 nm, h_{SiO2b} = 795 nm, h_{SiO2t} = 520 nm, t_{Au} = 600 nm. It is obtained by using finite element modelling software (Ansys HFSS). The propagation losses are dominated by the ohmic losses in the metallic strips (assuming gold conductivity $\sigma_{Au} = 4.1 \times 10^7$ S/m) calculated using the high-frequency skin depth approximation. The other materials are considered as lossless.

First, it is well known that membrane-supported CPW (shown in Fig. 3a) have much lower propagation loss than CPW on bulk substrate in the THz frequencies range because of their negligible radiation losses and lower effective index [25] [29] [30]. As it is shown in Fig. 3b, the odd mode of a MS-CPW with a slot width w_{slot} = 2 µm exhibits propagation losses (calculated by 2D finite element method using Ansys HFSS software) dominated by ohmic losses ($\sim\sqrt{f}$), which can be lower than 6 dB/mm at 1 THz. These theoretical results, which are well in agreement with experimental results (as it will be shown in the next part), show that we can expect a ~3-dB-power penalty for a 1-mm-long photomixer operating at ~1 THz. More importantly, the phase index of the fundamental mode of the CPW can be easily tuned to values lower than n_{φ}^{t} =2 (as shown in Fig 3c), close to the expected group index of a Si_3N_4/SiO_2 optical waveguide. In the following, we have set its characteristic impedance (Z_c) and slot width at Z_c =50 Ω and w_{slot}=2 µm. Obviously, the value of Z_c has been chosen in this study to be compatible with on-wafer-measurement set-up but could be set to different values (10 Ω <Z_c<500 Ω) if the photomixer was coupled to THz antennas. As for w_{slot} = 2 µm, this value is the result of a trade-off between the propagation loss which increases and the photoresponse which decreases (as shown in the following) with w. Furthermore, it is worth noting that the state of the art THz photomixers based on interdigitated electrodes patterned on LT-GaAs layers use 1.8-µm-interelectrode-spacing [12].

C. *Thermal management*

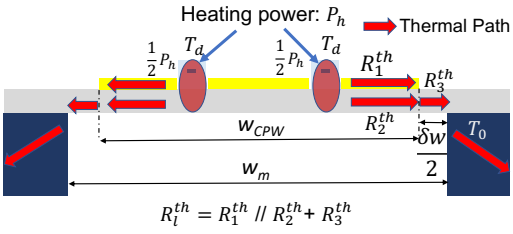

$$R_l^{th} = R_1^{th} \,//\, R_2^{th} + R_3^{th}$$

Fig. 4. Thermal model of travelling wave photomixer

GaAs membranes are widely used in the last stages of Schottky based THz multipliers and mixers [4] where the dissipated power is low (~mW) and the thermal management is not an issue. It is not the case here, where heating power density (joule heating and optical absorption) around 2 W per millimeter is expected. By assuming that the silicon bulk remains at room temperature, a thermal resistance per unit length R_{th}^{l} (see Fig. 4) not greater than 100 K/(W.m) is thus mandatory to achieve a maximum working temperature T_d~100 °C. A very loose estimation of R_{th}^{l} can be done by using a 1D model and by neglecting any thermal boundary ($\sigma_{LT-GaAs}^{th}$ = 25 W/(m·K), σ_{Au}^{th} = 317 W/(m·K)) [31] and the contribution of any bonding layer since direct GaAs/Si wafer bonding techniques have been already demonstrated [32] and could be eventually used to fabricate the device proposed here. By using dimensions given in Fig. 3a, it can be shown that R_{th}^{l}<100 K/(W.m) as long as the difference between the membrane width (w_m) and the total width of the CPW (w_s) δw < 2.5 µm. This result stems from the much better thermal conductance of the gold layer as compared with that of the LT-GaAs layer. This simple thermal model shows that a mm-long device can handle the watt power level only if membranes with limited widths are available. We will describe later the technological process allowing us to obtained membranes with transverse dimensions w_m< 100 µm, suitable for our application.

D. *Optical waveguide*

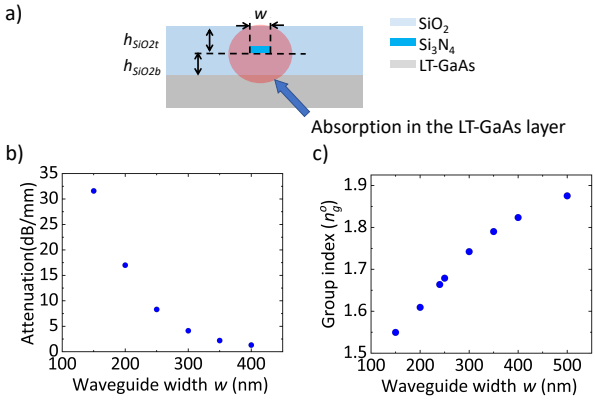

Fig. 5 a) Schematic of the SiO_2/Si_3N_4 IR waveguide b) optical absorption in the LT-GaAs and c) group index of the fundamental TE mode at λ=780 nm as a function of the core width w, w_{ground} = 6 µm, h_{SiO2b} = 795 nm, h_{SiO2t} = 520 nm. It is obtained by using a finite difference time domain method (using Lumerical software). Optical attenuation is linked to interband absorption in the LT-GaAs layer since the other materials are considered as lossless. Here the optical index used are n_{SiO2}=1.45, n_{Si3N4}=1.45 and $n_{LT\text{-}GaAs}$ = 3.70+0.09j [32].

The optical waveguide is described in Fig.5a. It consists of a 200-nm-thick silicon nitride core embedded in silicon oxide cladding laying on a LT-GaAs absorbing layer. The absorption in this latter is dependent on the overlap of the fundamental TE optical mode with the LT-GaAs layer and can be tuned by varying the width (w) of the silicon nitride core. In Fig. 5b and Fig. 5c are plotted the calculated group index and optical losses (only due to the absorption in the LT-GaAs layer here since the other media are assumed to be lossless) of the fundamental TE-mode as a function of the waveguide width (see Fig.5 caption for structure details). It can be seen that the core width can be tuned in order to have in principle a complete absorption of the optical input power within the 1-mm-length of the proposed device and a group index close to the effective index of the CPW mode. Furthermore, we can take advantage of the dependence of the absorption in the LT-GaAs layer on the waveguide width to achieve a linear decrease of the optical

power along the device (instead of exponential) and avoid any power limitation due to a thermal failure at its very beginning (see appendix A).

III. OPTOELECTRONICS MODEL

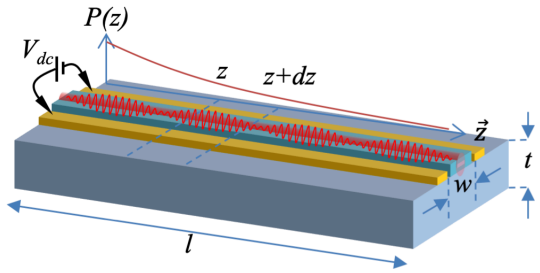

Fig. 6. Schematic of the travelling wave photoconductor under study

Optoelectronics modeling of the travelling wave photomixer is not dependent on the THz waveguide, therefore, for simplicity, we are going to carry out this model by studying the simplest version of a distributed photoconductor consisting of a coplanar strip waveguide patterned on a LT-GaAs epitaxial layer as shown in Fig. 6. In this part, we have improved and adapted to our device the model developed in ref. [19]. Furthermore, we have developed, in appendix A, a simple model allowing for a better understanding of the effect of the backwards photocurrent on the frequency response of a TW photomixer.

A. *Optical pump*

Let us consider the optical waveguide coupled slightly to the LT-GaAs layer as shown in Fig. 6, whose fundamental mode has a propagation constant along the z axis $\beta(\omega)$ (see Fig. 6 for details) and an absorption coefficient α_o stemming from the absorption in the LT-GaAs layer. Let us assume two slightly detuned CW laser beams of angular frequency ω_1 and ω_2 of same power ($P_0/2$) and polarization injected in the dielectric waveguide. This results in an optical power $P(z,t)$ as detected by an ultrafast photodetector which can be expressed by [19]:

$$P(z,t) = P_0[1 + \cos(\omega_b t - (\beta(\omega_1) - \beta(\omega_2))z]e^{-\alpha_o z} \quad (2)$$

Here, it is worth noting that the parts of the energy flow oscillating at angular frequency $\omega_1 + \omega_2$ (optical range) much larger than the photoconductor cut off frequency (in the THz range) is canceled because of the time averaging. By using a Taylor expansion of the optical mode dispersion characteristics $\beta(\omega)$, we obtain:

$$\beta(\omega_1) - \beta(\omega_2) \approx \frac{d\beta}{d\omega}(\omega_1 - \omega_2) \quad (3)$$

with $\frac{d\beta}{d\omega} = \frac{1}{v_g^o}(\omega_1 - \omega_2) = \frac{n_g^o}{c}\omega_b$. In the following, we set $k_o = n_g^o \omega_b c$. The optical power in the guide can be finally expressed as follows:

$$P(z,t) = P_0[1 + \cos(\omega_b t - k_o z)]e^{-\alpha_o z} \quad (4)$$

which can be split in two terms $P(z,t) = P_{dc}(z) + P_1(z,t)$ where $P_{dc}(z) = P_0 e^{-\alpha_o z}$ and $P_1(z,t) = P_0 \cos(\omega_b t - k_o z)e^{-\alpha_o z}$. The oscillating part at ω_b, can be expressed in the phase vector notation:

$$P_1(z,t) = Re(P_{ac}(\omega_b, z)e^{j\omega_b t}) \quad (5)$$

with $P_{ac}(\omega_b, z) = P_0 e^{-\alpha_o z}e^{-jk_o z}$.

B. *Photocurrent source*

Now, if we consider a photoconductor consisting of two metallic bias electrodes patterned on a low-carrier lifetime photoconductive material of thickness t (carrier lifetime τ, mobility μ, dc bias electric field magnitude $E_{dc} << E_s$ the saturation velocity electric field) separated from a distance w, we can easily evaluate the oscillating part of the maximum photocurrent $dI_{ac}(\omega_b, z)$ generated between z and $z + dz$ by using the basic photoconduction theory for carrier lifetime-limited ultrafast photoconductors [33] [15]:

$$dI_{ac}(\omega_b, z) = -\frac{q}{\hbar\omega}\frac{(|P_{ac}(z+dz)| - |P_{ac}(z)|)}{\sqrt{1+(\omega_b\tau)^2}}\frac{\tau}{\tau_{tr}}e^{-j\varphi}e^{-jk_o z} \quad (6)$$

where $\omega = \frac{\omega_1+\omega_2}{2}$, $\varphi = tan^{-1}(\omega_b\,\tau)$ and $\tau_{tr} = w/(\mu E_{dc})$ (assuming a 1D photoconductor), hence, by using a first order Taylor expansion, we obtain:

$$\frac{dI_{ac}(\omega_b, z)}{dz} = -\frac{q}{\hbar\omega}\frac{1}{\sqrt{1+(\omega_b\tau)^2}}\frac{d|P_{ac}(z)|}{dz}\frac{\tau}{\tau_{tr}}e^{-j\varphi}e^{-jk_o z} = A(\omega_b)e^{-\gamma_o z} \quad (7)$$

with $A = \alpha_o P_0 \frac{q}{\hbar\omega}\frac{1}{\sqrt{1+(\omega_b\tau)^2}}\frac{\tau}{\tau_{tr}}e^{-j\varphi}$ and $\gamma_o = jk_o + \alpha_o$. Furthermore, it is known from the small signal electrical model of a photomixing source [34] that this photocurrent source has an internal admittance $G_0\,dz$ expressed as follows:

$$G_0 dz \approx -\frac{q}{\hbar\omega}\frac{\mu\tau}{w^2}(P_{dc}(z+dz) - P_{dc}(z)) \quad (8)$$

Hence, the internal admittance per unit length is:

$$G_0 \approx -\frac{q}{\hbar\omega}\frac{\mu\tau}{w^2}\frac{dP_{dc}}{dz} \approx \alpha_o P_0 \frac{q}{\hbar\omega}\frac{\mu\tau}{w^2}e^{-\alpha_o z} \quad (9)$$

C. *Distributed equivalent circuit model*

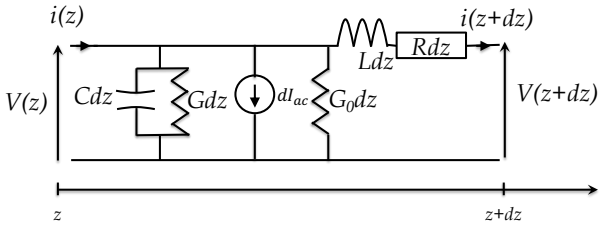

Fig. 7. Equivalent transmission line modelling a photomixer

A TW photomixer can be modeled as a standard transmission line having a distributed photocurrent source $\frac{dI_{ac}}{dz}$ of internal admittance per unit length G_0 calculated in the previous section (see Fig. 7). Assuming voltage waves of the form $V_s(z,t) = Re(V(z)e^{j\omega_b t})$, it can be found that $V(z)$ is a solution of the differential equation [19]:

$$\frac{d^2V}{dz^2} = V(z) \times Z(Y + G_0) + Z\frac{dI_{ac}}{dz} \quad (10)$$

where $Z = R + jL\omega_b$ and $Y = G + jC\omega_b$. Here, Z and Y are related to the THz waveguide without any source (see

appendix B). Here, G~0 since propagation losses related to the dielectric loss and free carrier absorption are negligible in the LT-GaAs. We assume than G_0 is much smaller than Y, we obtain finally the standard telegrapher's differential equation with a current source term:

$$\frac{d^2V}{dz^2} - \gamma_t{}^2 V(z) = +ZAe^{-\gamma_o z} \tag{11}$$

with $\gamma_t = \sqrt{ZY} = jk_t + \alpha_t/2$.

TABLE I
NUMERICAL VALUES USED IN THE OPTOELECTRONICS MODEL

Symbol	Quantity	Value
L	Photomixer length	1 mm
w	electrode spacing	2 µm
τ	carrier lifetime	0.5 ps
v_s	Saturation velocity	8×10^6 cm/s [35]
E_s	Saturation field	~50 kV/cm
µ	carrier mobility	~200 cm^2/(V.s) [36]
$\hbar\omega$	photon energy	1.58 eV (λ=780 nm)
α_o	absorption coefficient	2.3 mm^{-1} (10 dB/mm)
Z_c	Characteristic Impedance	50 Ohm
n_φ^t	THz effective mode index	1.8

By using the typical values shown in Table 1, we should obtain at an optical power P_0 = 2 W which should be handled by a 1 mm-long TW photomixer a maximum internal admittance, G_0 = 7.3 S/m and a maximum photocurrent per unit length dI_{ac}/dz = 58.2 A/m. The capacitance and inductance of a THz waveguide of n_φ^{THz} and Z_c given in Table 1 are L = 0.3 µH/m, C = 120 pF/m. It shows that $|Y| = |jC\omega_b| > 10G_0$ as soon as $f_b \approx$ 100 GHz. The solutions of (11) are:

$$V(z) = V_1 e^{-\gamma_t z} + V_2 e^{\gamma_t z} + \frac{ZA}{\gamma_o^2 - \gamma_t^2} e^{-\gamma_o z} \tag{12}$$

$$I(z) = \frac{V_1}{Z_c} e^{-\gamma_t z} - \frac{V_2}{Z_c} e^{\gamma_t z} + \frac{\gamma_o ZA}{\gamma_o^2 - \gamma_t^2} e^{-\gamma_o z} \tag{13}$$

where V_1 and V_2 are integration constants given by the boundary conditions. As it will be shown in the next section, the boundary conditions in our device will be an open circuit input termination and a match load output, i.e.: $I(0) = 0$ and $V(L)/I(L) = Z_c$. Once the $V(z)$ is calculated by using (12), (13) and the boundary conditions given above, the THz output power delivered to a load of impedance Z_l is calculated by:

$$P_{THz} = \frac{1}{2} Re\left(\frac{1}{Z_l}\right)|V(L)|^2 \tag{14}$$

In Fig.8 are plotted the THz output power as a function of frequency calculated by using this model when the optical power P_0 = 2 W. Three different index differences $\Delta n = |n_\varphi^t - n_g^o|$ have been considered here with α_o=10 dB/mm: Δn=0, 0.13 and 0.2. For comparison, we have also plotted the first two Δn values when α_o increases along the device so that the optical power decreases linearly, i.e. dP_0/dz is constant. The other parameters used in the simulation are given in Table 1 and the device input termination is an open circuit. It can be seen that for perfect phase matching, output powers reaching 200 µW at 1 THz and 3 µW at 4 THz are expected with this device. However, it is obvious that if the optical pump is absorbed in the device according an exponential law, it will hamper the optical power handling capabilities of the device. We have also plotted in Fig. 8 the results obtained when the optical pump decreases linearly along the waveguide (see Appendix A for further details):

$$-\frac{d|P_{ac}(z)|}{dz} = \frac{P_0}{L} \tag{15}$$

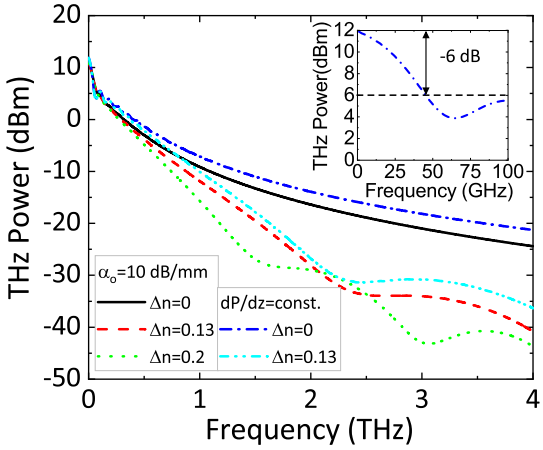

Fig. 8. Theoretical THz power as a function of the beating frequency provided to a 50 Ohm load by a 1-mm-long TW photomixer pumped by an optical beatnote of power P_0=2 W. The average photocurrent is I_{dc} =22.5 mA. Inset: Closeup showing the low frequency part of the plot where happens the 6-dB-roll-off related to the large phase-mismatch experienced by the backward photocurrent waves (half the total photocurrent, see Annexe A). It can be seen as the signature of a travelling wave behavior.

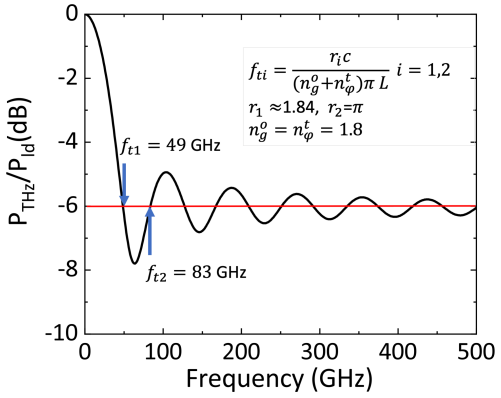

Fig. 9. Theoretical power provided by lossless 1-mm-long TW photomixer (α_t = 0) normalized to the power provided by a perfect (no RC cut off frequency) lumped device P_{THz}/P_{Id}. Here is assumed a linear absorption of the optical power. In the inset are shown the analytic expression of f_{t1}, f_{t2} as demonstrated in appendix B.

In this case, the expected power level is very similar. Practically, the optical waveguide width will be designed so that $\alpha_o(z)$ decreases when z increases. We can point out that when Δn =0.13, we find effectively the 3-dB-power penalty previously calculated using the simplified model presented in Appendix B. Furthermore as previously seen in [19] and as shown in the inset of Fig. 8, the travelling wave signature of a photodetector is a 6 dB loss in the frequency response at "low" frequency as compared with a lumped device photomixer at equal photocurrent. It occurs when the contribution of the backward photocurrents is canceled because of the large phase-mismatch with the input optical wave. We have shown in Fig. 9 the frequency dependence of the THz power provided by a lossless ($\alpha_t = 0$) 1-mm-long TW photomixer normalized to the power provided by a hypothetical lumped device (size<<λ_t) at equal photocurrent level. We have also shown the two first frequencies f_{t1}, f_{t2} at which the 6 dB-power penalty occurs, which can be

calculated analytically and are inversely proportional to $L(n_g^o + n_\varphi^t)$ (see Appendix B and Fig.9 for further details). A photoconductor working in a TW regime should thus exhibit a frequency response presenting a 6-dB roll-off at frequencies close to f_{t1}, f_{t2} followed by a plateau-like response. We will see in the next part that the TW photomixers characterized in this study present clearly this TW-like frequency response unlike the previous attempts.

IV. FABRICATION

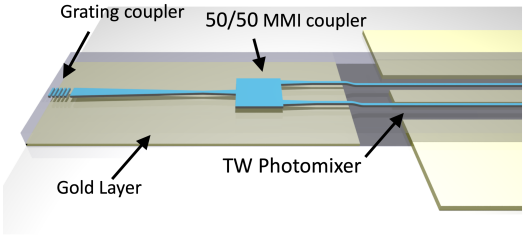

Fig. 10. Schematic of the whole device including the grating coupler and the MMI coupler aimed at pumping equally the two slots of the CPW.

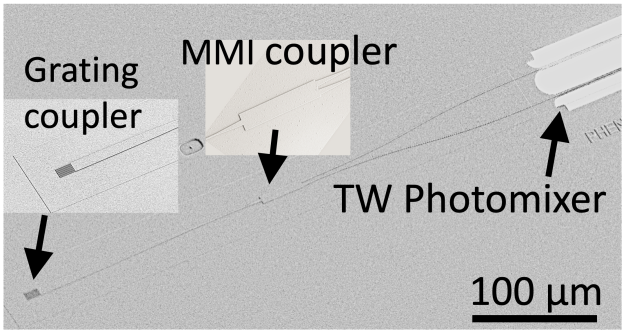

Fig. 11. SEM picture of the entire device including the grating coupler and the 50/50 MMI coupler allowing for pumping the two-slots TW photomixer.

A. Low temperature fabrication process of Si_3N_4/SiO_2 optical waveguides

The entire device, as shown in Fig. 10 and Fig. 11, besides the LT-GaAs membrane-supported TW photomixer, consists of a grating coupler and a 50/50 MMI coupler [37] in order to pump equally each slot of the CPW. The watt-level optical power considered in the previous part is indeed not compatible with the standard butt coupling through a cleaved facet used to couple the light coming from a SM optical fiber to a TW photodetector as it was done in the previous attempts using semiconductor-based optical guides. Grating couplers, widely studied in recent years [38] [39], are obviously more suitable to high pump power devices. We have developed an optical waveguide platform for visible and infrared wavelengths using Si_3N_4/SiO_2 layers deposited at low temperature (~300 °C) compatible with III-V semiconductors by using plasma enhanced chemical vapor deposition (PECVD) technique with optimized process parameters [40]. Furthermore, as shown in Fig. 10, a thin gold layer (70 nm) is sandwiched between the semiconductor and the dielectric optical waveguide to obtain a high efficiency grating coupler (by using the gold layer as reflecting mirror) and to avoid optical absorption in the semiconductor layer until the beginning of the active device. We have measured, on optical waveguides fabricated by using this fabrication process, propagation losses around 0.5 dB/mm and coupling loss CL~3 dB at a wavelength λ=780 nm [41]. It is worth noting that the coupling loss is not optimized since theoretical calculations predict CL~1 dB. In addition, propagation losses are compatible with our application since the distance between the grating coupler and the beginning of the device is smaller than 0.5 mm (as shown Fig11). Last, the 50/50 MMI coupler, optimized by using a 3D finite difference beam propagation method [42] shows very encouraging experimental insertion loss IL~3.5 dB on each output branch.

B. LT-GaAs narrow membrane fabrication

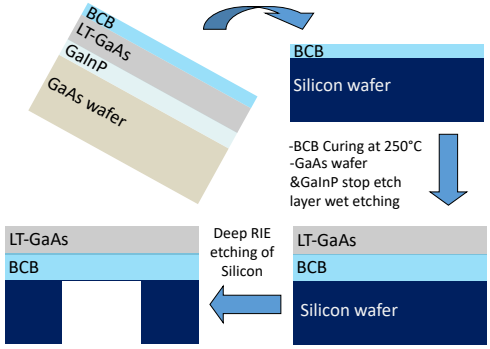

Fig. 12. Schematic of the narrow LT-GaAs membrane fabrication process. BCB layer thickness: 200 nm.

Narrow (<100 µm) LT-GaAs membrane have been fabricated thanks to the process described in Fig.12. In a first step, a layer transfer process using a 200-nm-thick-benzocyclobutene (BCB) polymer layer is used to bond the LT-GaAs layer on a high-resistivity silicon wafer [43]. Then, narrow LT-GaAs membranes are patterned by etching the silicon wafer (thickness~200µm) by means of Bosch process deep reactive ion etching (see [44] for example). In Fig 13 is shown a SEM view of a cross section of 45-µm-wide LT-GaAs membrane-supported photomixer including the optical waveguide patterned within the CPW slots. It is worth noting that the additional thermal resistance due to the additional BCB layer is assumed to be negligible since the low thermal conductivity ($\sigma_{BCB}^{th} = 0.3\ \mathrm{W{\cdot}m^{-1}{\cdot}K^{-1}}$ [45]) of BCB is mitigated by the sub-micrometer layer thickness, which could be further reduced, if needed, by optimizing the fabrication process.

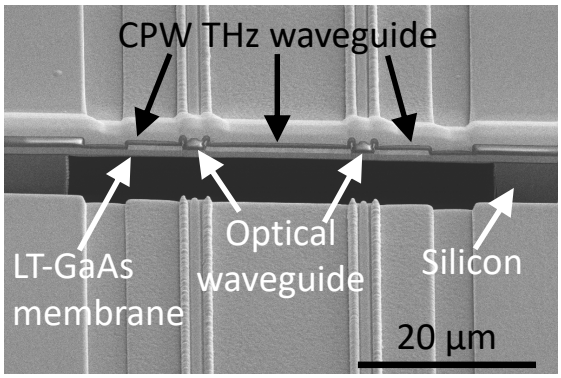

Fig. 13. SEM view of a FIB-cut cross section of the membrane-supported TW photomixer.

V. CARACTERIZATION

A. LT-GaAs membrane-supported CPW

On-wafer-characterization of the THz waveguides has been performed up to 750 GHz by using a vector network analyser with five different frequency extenders and coplanar probes. We extracted waveguide propagation constants from scattering matrix measurements performed on waveguides with different lengths [46] to mitigate the errors induced during the calibration process by the use of impedance standard substrates (3 different substrates depending of the frequency bands) provided by the probes suppliers instead of on-wafer standards. We present in the left panel of Fig 14 the experimental attenuation coefficients of a 1-µm-thick membrane-supported CPW. It can be noticed a rather good agreement with the theoretical results obtained by FEM modelling (assuming an infinitely wide membrane). However, the surface impedance approximation used in the FEM model gives only a rough estimation of ohmic losses which dominate the propagation losses of the membrane supported CPW since the radiation losses are almost canceled. We have also plotted in Fig 14, theoretical ohmic losses obtained by using a quasi-TEM model of coplanar waveguides developed by Heinrich [47]. This model assumes an infinitely thick substrate and we mimicked a membrane-supported CPW by setting the dielectric constant of the substrate ϵ_r so that the quasi-TEM effective dielectric constant of the CPW TEM mode n_φ^t is close to that obtain by the FEM model ($n_\varphi^t \approx 2$). In the quasi-static limit, the effective index n_φ^t of a CPW patterned on a substrate of dielectric constant ϵ_r is given by $n_\varphi^{t\,2}=(\epsilon_r+1)/2$, thereby if $n_\varphi^t=2$, $\epsilon_r=7$. It can be noticed a very good agreement of the propagation loss given by this model with the experimental ones at least from 1 to 500 GHz.

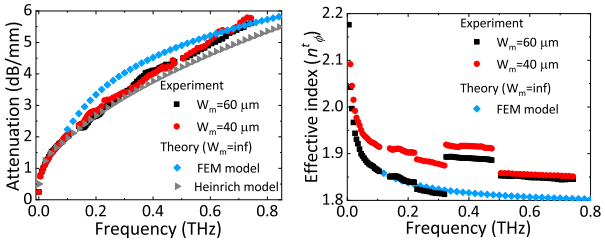

Fig. 14 THz attenuation α_t and effective index n_φ^t, as function of frequency on a LT-GaAs membrane-supported CPW without optical waveguide. Geometrical parameters: w_m=40 and 60 µm, w_{strip}=6 µm, w_{ground}=10 µm, and w_{slot}=2 µm. Theoretical values have been obtained by FEM modelling (see inset of Fig. 3 for further details) and by using a quasi_TEM model [47]. Experimental values have been obtained by using scattering parameters measurements on CPW of two different lengths L_1=1 mm and L_2=4 mm [46].

The 40 µm-width membrane show similar attenuation coefficient as the 60µm-width, around 5.5 dB/ mm at 750 GHz, values still acceptable for a 1-mm-length TW photomixer. Regarding the effective index n_φ^t plotted in the right panel of Fig. 14, which is extracted from phase measurements, extremely sensitive to exact probes distances and calibration, experimental values are clearly less reliable at frequency greater than 300 GHz. At higher frequency, we can estimate by comparison with experimental results obtained at lower frequency and also with simulations that the error in phase measurement results in a relative error in the determination of the effective index $\Delta n_\varphi^t/n_\varphi^t \approx \pm 3\%$. Though, we can still conclude that effective index well below n_φ^t=1.9 are achievable with this technology but also that narrower membranes exhibit higher effective index which can be explained by a slight overlap of the CPW mode and the silicon substrate.

B. 1-mm-long TW photomixer: frequency response

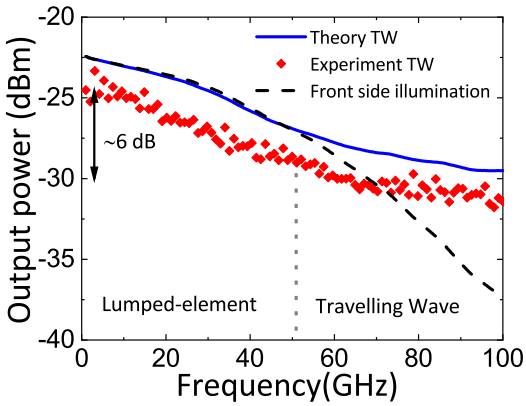

Fig. 15: Theoretical (line) and experimental (symbols) electrical response of a 1-mm-long TW photomixer at 10 V bias and an optical power P_0=0.4 W resulting in a dc photocurrent I_{dc}=0.5 mA. The theoretical values are obtained by using the model presented previously assuming $n_g^o = 1.8$ and $\alpha_o = 10$ dB/mm whereas the other input parameters have been measured ($n_\varphi^t \approx 2$, $Z_c \approx 50$ ohm, $\tau \approx 0.5$ ps, etc.). However A(ω=0) is calculated from I_{dc}. In dash line is also plotted the theoretical output power assuming a front side illumination (obtained by using our model with $n_\varphi^t = 0$).

On-wafer electrical characterization of a 1 mm-long-TW photomixer has been performed up to 100 GHz by using a 780-nm Toptica TeraScan system and a Toptica 780-nm SOA amplifier. The device is illuminated by the optical beatnote through a cleaved-fiber and the output power is collected by using a coaxial-coplanar probe and sent to a thermal power sensor (R&S®NRP-Z58). Fig. 15 shows the frequency response of the device up to 100 GHz. First of all, it should be noticed that the output power is very low despite a very large optical pump (maximum P_0 =400 mW, limited by our set-up) due to a very low photoresponse (S=1.25 mA/W) and dc photocurrent (I_{dc}=0.5 mA) on this sample which is likely to be related to technological issues which could be easily resolved in future fabrication runs. A photoresponse S =13 mA/W has been indeed measured on TW photomixers aimed at dc measurements (with only one slot instead of two slots) which is comparable to the photoresponse obtained on planar photoconductor based on LT-GaAs [12]. However, the experimental frequency response reveals clearly a transition between a lumped-element and a traveling behavior around 50 GHz, as expected in our simplified model. We have also plotted the theoretical response using the model developed in this study which is in good agreement with the experience. Lastly, the theoretical frequency response in the case of a front side illumination is shown in order to spotlight the deleterious effect of the phase mismatch between optical and THz waves for large size photomixers.

VI. CONCLUSION

A TW photomixer based on a Si_3N_4/SiO_2 optical waveguide coupled to LT-GaAs membrane-supported CPW has been designed, fabricated and characterized. This topology, by allowing for a quasi-perfect phase matching between the optical pump and the emitted THz waves opens the way to photomixing sources with mW power level below 1 THz and µW power level up to 4 THz. In this study, a genuine

travelling-wave behavior has been demonstrated as a first step toward photomixers with unprecedented performance. Recent promising optimization of the absorption of 1550-nm light in LT-GaAs [48] give us hope that this concept could be also promising to develop TW photomixers pumped by low-cost and powerful 1550-nm fiber lasers and amplifiers.

APPENDIX A: DESIGN OF THE OPTICAL WAVEGUIDE TO ACHIEVE A LINEAR DECREASE OF THE OPTICAL POWER

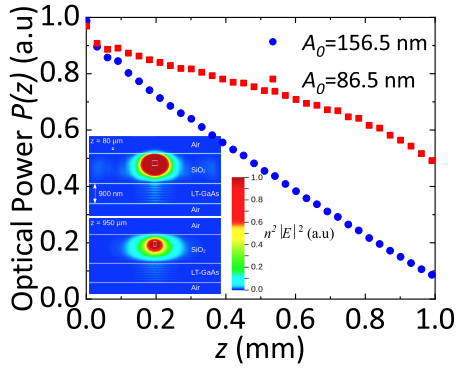

Fig. A1. Calculation by means of 3D beam propagation method of the optical power carried by the fundamental TE mode (as described in Fig. 5.a) with a varying width *w(z)* as given in Eq. A5. Inset: Square of the electric field strength times the optical index after propagation lengths of 80 µm and 950 µm. We can notice that, thanks to the different waveguide's widths, the amplitude of the stationary waves in the GaAs have values quite similar in both cases resulting in a similar linear absorption.

A linear decrease of the optical power along the waveguide *P(z)* is thus given, in the case of a photoconductor of length (*L*) pumped by an input optical power P_0, by:

$$P(z) = P_0\left(1 - \frac{z}{L}\right) \tag{A1}$$

In order to design this linear decrease, one possible way is to find a position-dependent absorption coefficient $\alpha(z)$ such as:

$$P_0\left(1 - \frac{z}{L}\right) = P_0 e^{-\alpha(z)z} \tag{A2}$$

Thereby,

$$\alpha(z) = -\frac{1}{z} ln\left(1 - \frac{z}{L}\right) \tag{A3}$$

By using the dependency of the absorption in the GaAs on the width of the waveguide (*w*), which can be approximated (by using the data shown in Fig. 5b) by:

$$w(|\alpha|) = Ae^{-\frac{|\alpha|}{t_1}} + A_0 \tag{A4}$$

with *w, A, A_0* given in nm and $|\alpha|$ in dB/mm. The best fit is obtained by setting *A*=272.5 nm, A_0=156.5 nm and t_1=7.5 dB/mm. By using the two last equations, we obtain w(z):

$$w(z) = Ae^{-\frac{10log\,(e)}{t_1 L}} + A_0 \tag{A5}$$

We show in Fig. A1 the optical power $P(z)$ calculated by using a 3D finite difference beam propagation method [42] for a waveguide width *w(z)* as defined above and after optimization (A_0=86.5 nm instead of 156.5 nm). The near perfect linear decrease of the optical power in the latter case obtained by a 3D simulation method shows the validity of our semi-analytic method and that photoconductors with watt level input power is feasible.

APPENDIX B: SIMPLIFIED MODEL OF THE TRAVELLING WAVE PHOTOMIXER

In this model, we study a travelling wave photomixer based on a coplanar waveguide of length L and characteristic impedance Z_c. We assume that the absorption coefficient of the optical waveguide is a function of z, $\alpha_o(z)$ such as the photocurrent amplitude generated along the path of the optical beam is constant along the photodetector:

$$-\frac{d|P_{ac}(z)|}{dz} = \frac{P_0}{L} \tag{B1}$$

Hence, the THz current created in z is:

$$dI_{ac}(z) = Je^{-jk_o z}dz \tag{B2}$$

where $J = -\frac{P_0}{L}\frac{q}{\hbar\omega}\frac{1}{\sqrt{1+(\omega_b\tau)^2}}\frac{\tau}{\tau_{tr}}e^{-j\varphi}$ is homogeneous to a current per unit length. In addition, let us assume that the device is closed at its both ends with a perfect match resistor ($R = Z_c$). If we are focused on the power dissipated only in the output resistor, we can consider only the forward waves at the output of the device ($z = L$). The forward THz current created in z_0, $\frac{1}{2}dI_{ac}(z)$ travels without loss, on the CPW guide at a phase velocity $v_\varphi^t = c/n_\varphi^t$ and a wavelength number k_{THz} and give a contribution to the total output current $dI_{ac\_L}(z)$:

$$dI_{ac\_L}(z) = \frac{1}{2}dI_{ac}(z)e^{-jk_t(L-z)} \tag{B3}$$

the total current at the output I_{total} is:

$$I_{total} = \int_0^L dI_{ac\_L}(z) = \frac{1}{2}Je^{-jk_tL}\int_0^L e^{j\Delta k\, z}dz$$
$$= \frac{1}{2}LJe^{-jk_tL}e^{-jL\Delta k/2}\frac{\sin L\Delta k/2}{L\Delta k/2} \tag{B4}$$

with $\Delta k \equiv k_t - k_o = \omega_b/c\,(n_g^t - n_\varphi^o)$. The THz output power P_{THz} delivered to the load Z_c is then given by $P_{THz} = 1/2\,Z_c|I_{total}|^2$ whose maximum $P_{mf} = 1/8\,Z_c|LJ|^2$ is obtained when Δk=0. It is worth noting that only a quarter (-6 dB) of the power obtained with a lumped device exhibiting the same dc-photocurrent $P_{ld} = 1/2\,Z_c|LJ|^2$. Furthermore, the loss induced by the phase mismatch $L_{\Delta\varphi}$is thus identical to the one experienced in THz emission based on non-linear process:

$$L_{\Delta\varphi} = \frac{P_{THz}}{P_{mf}} = \left|\frac{\sin L\Delta k/2}{L\Delta k/2}\right|^2 \tag{B5}$$

Now, if we assume an open circuit at the device input ($Z_{input} \approx +\infty$), we have to add the effect of the backward photocurrent waves after they have been reflected at the input. The contribution of the photocurrent generated between *z* and *z+dz* to the total output becomes:

$$dI_{ac\_L}(z) = \frac{1}{2} dI_{ac}(z) e^{-jk_t(L-z)} + \frac{1}{2} dI_{ac}(z) e^{-jk_t(L+z)} \quad \text{(B6)}$$

And the total current at the output I_{total} is given by:

$$I_{total} = \frac{1}{2} LJ e^{-jk_t L} \left(e^{jL\Delta k/2} \frac{\sin L\Delta k/2}{L\Delta k/2} + e^{-jL\Sigma k/2} \frac{\sin L\Sigma k/2}{L\Sigma k/2} \right) \quad \text{(B7)}$$

with $\Sigma k \equiv k_o + k_t = \frac{\omega_b}{c}(n_g^o + n_\varphi^t)$. In order to help for the interpretation of the results obtained in Fig. 8, let us assume that $n_g^o = n_\varphi^t \approx 1.8$ and thus $\Delta k \approx 0$ and $\Sigma k \approx 3.6$. The output power may now be expressed as follows:

$$P_{THz} = \frac{1}{4} P_{ld} \left| 1 + e^{-jL\Sigma k/2} \frac{\sin L\Sigma k/2}{L\Sigma k/2} \right|^2 \quad \text{(B8)}$$

This time, at $\omega \approx 0$, $P_{THz} \approx P_{ld}$ and $P_{THz} \approx 1/4\, P_{ld}$ when $\omega \to \infty$ after some ripples, since the second term in (B8) becomes rapidly negligible when the frequency increases because of the huge phase mismatch of the backward wave with the optical pump. P_{THz} is equal to $1/4\, P_{ld}$ as soon as the second term in (B8) is equal to unity. The two first intersection frequencies f_{t1}, f_{t2} are obtained when $L\Sigma k/2 \approx 1.84$ and $L\Sigma k/2 = \pi$, respectively, i.e f_{i1}=49 GHz and f_{i2}=83 GHz.

APPENDIX C: THZ WAVEGUIDE WITHOUT SOURCE

In this case, we find the standard telegrapher's equation whose general solutions are voltage and current waves which are propagating on a transmission line are:

$$V(z) = V_1 e^{-\gamma_t z} + V_2 e^{\gamma_t z} \quad \text{(C1)}$$

$$I(z) = \frac{V_1}{Z_c} e^{-\gamma_t z} - \frac{V_2}{Z_c} e^{+\gamma_t z} \quad \text{(C2)}$$

where $Z_c = \frac{Z}{\gamma_t} = \sqrt{\frac{Z}{Y}}$. It can be easily shown, for the low-loss CPW studied here in which $R \ll L\omega_b$ and $G \approx 0$, that $Z_c \approx \sqrt{L/C}$ and $\gamma_t = j\omega_b\sqrt{LC} + R/2Z_c$. Furthermore, if we set $\gamma_t = jk_t + 1/2\alpha_t$, it gives $k_t \approx j\omega_b\sqrt{LC}$ and $R/Z_c \approx \alpha_t$. The elementary components of the transmission line L,C and R are thus related to Z_c, n_φ^t and α_t as follows:

$$C \approx \frac{n_\varphi^t}{cZ_c}, \quad L \approx \frac{Z_c\, n_\varphi^t}{c}, \quad R \approx Z_c \alpha_t \quad \text{(C3)}$$

REFERENCES

1. E. Brown and K. McIntosh, "Photomixing up to 3.8 THz in low-temperature-grown GaAs," Appl. Phys. Lett. **66**, 285–287 (1995).
2. T. Nagatsuma, "Generating millimeter and terahertz waves," IEEE Microw. Mag. **10**, 64–74 (2009).
3. S. Preu, G. H. Döhler, S. Malzer, L. J. Wang, and A. C. Gossard, "Tunable, continuous-wave Terahertz photomixer sources and applications," J. Appl. Phys. **109**, 061301 (2011).
4. G. Chattopadhyay, "Technology, Capabilities, and Performance of Low Power Terahertz Sources," IEEE Trans. Terahertz Sci. Technol. **1**, 33–53 (2011).
5. L. Liebermeister, S. Nellen, R. Kohlhaas, S. Breuer, M. Schell, and B. Globisch, "Ultra-fast, High-Bandwidth Coherent cw THz Spectrometer for Non-destructive Testing," J. Infrared, Millimeter, Terahertz Waves 1–9 (2019).
6. A. Roggenbuck, H. Schmitz, A. Deninger, I. C. Mayorga, J. Hemberger, R. Güsten, and M. Grüninger, "Coherent broadband continuous-wave terahertz spectroscopy on solid-state samples," New J. Phys. **12**, 043017 (2010).
7. T. Nagatsuma, G. Ducournau, and C. C. Renaud, "Advances in terahertz communications accelerated by photonics," Nat. Photonics **10**, 371–379 (2016).
8. E. Peytavit, S. Lepilliet, F. Hindle, C. Coinon, T. Akalin, G. Ducournau, G. Mouret, and J.-F. Lampin, "Milliwatt-level output power in the sub-terahertz range generated by photomixing in a GaAs photoconductor," Appl. Phys. Lett. **99**, 223508 (2011).
9. T. Ishibashi, Y. Muramoto, T. Yoshimatsu, and H. Ito, "Unitraveling-Carrier Photodiodes for Terahertz Applications," IEEE J. Sel. Top. Quantum Electron. **20**, 79–88 (2014).
10. E. Rouvalis, C. C. Renaud, D. G. Moodie, M. J. Robertson, and A. J. Seeds, "Continuous Wave Terahertz Generation From Ultra-Fast InP-Based Photodiodes," IEEE Trans. Microw. Theory Tech. **60**, 509–517 (2012).
11. I. D. Henning, M. J. Adams, M. Vaughan, T. Abraham, Y. Sun, A. Dyson, D. G. Moodie, D. C. Rogers, P. J. Cannard, S. Dosanjh, M. Skuse, and R. J. Firth, "Novel Antenna-Integrated Photodiodes With Strained Absorbers Designed for Use as Terahertz Sources," J. Sel. Top. quantum Electron. 1–8 (2010).
12. S. M. Duffy, S. Verghese, K. A. Mcintosh, A. Jackson, A. C. Gossard, and S. Matsuura, "Accurate modeling of dual dipole and slot elements used with photomixers for coherent terahertz output power," IEEE Trans. Microw. Theory Tech. **49**, 1032–1038 (2001).
13. C. C. Renaud, M. Natrella, C. Graham, J. Seddon, F. Van Dijk, and A. J. Seeds, "Antenna Integrated THz Uni-Traveling Carrier Photodiodes," IEEE J. Sel. Top. Quantum Electron. **24**, 1–11 (2018).
14. H. Ito, T. Furuta, S. Kodama, and T. Ishibashi, "InP/InGaAs uni-travelling-carrier photodiode with 310 GHz bandwidth," Electron. Lett. **36**, 1809 (2000).
15. E. Peytavit, M. Billet, Y. Desmet, G. Ducournau, D. Yarekha, and J.-F. Lampin, "THz photomixers based on nitrogen-ion-implanted GaAs," J. Appl. Phys. **118**, 183102 (2015).
16. J. Soohoo, Shi-Kay Yao, J. E. Miller, R. R. Shurtz, Yuan Taur, and R. A. Gudmundsen, "A Laser-Induced Traveling-Wave Device for Generating Millimeter Waves," IEEE Trans. Microw. Theory Tech. **29**, 1174–1182 (1981).
17. H. F. Taylor, O. Eknoyan, C. S. Park, K. N. Choi, and K. Chang, "Traveling Wave Photodetectors," in *OE/LASE '90, 14-19 Jan., Los Angeles, CA*, A. Katzir, ed. (1990), pp. 59–63.
18. K. S. Giboney, R. L. Nagarajan, T. E. Reynolds, S. T. Allen, R. P. Mirin, M. J. W. Rodwell, and J. E. Bowers, "Travelling-Wave Photodetectors with, 172-GHz Bandwidth and 76-GHz Bandwidth-Efficiency Product," IEEE Photonics Technol. Lett. **7**, 412–414 (1995).
19. V. M. Hietala, G. A. Vawter, T. M. Brennan, and B. E. Hammons, "Traveling-wave photodetectors for high-power, large-bandwidth applications," IEEE Trans. Microw. Theory Tech. **43**, 2291–2298 (1995).
20. L. Y. Lin, M. C. Wu, T. Itoh, T. A. Vang, R. E. Muller, D. L. Sivco, and A. Y. Cho, "Velocity-matched distributed photodetectors with high-saturation power and large bandwidth," IEEE Photonics Technol. Lett. **8**, 1376–1378 (1996).
21. L. Y. Lin, M. C. Wu, T. Itoh, T. A. Vang, R. E. Muller, D. L. Sivco, and A. Y. Cho, "High-power high-speed photodetectors-design, analysis, and experimental demonstration," IEEE Trans. Microw. Theory Tech. **45**, 1320–1331 (1997).
22. E. Dröge, E. H. Böttcher, S. Kollakowski, A. Strittmatter, D. Bimberg, O. Reimann, and R. Steingrüber, "78 GHz distributed InGaAs MSM photodetector," Electron. Lett. **34**, 2241 (1998).
23. Yi-Jen Chiu, S. B. Fleischer, and J. E. Bowers, "High-speed low-temperature-grown GaAs p-i-n traveling-wave photodetector," IEEE Photonics Technol. Lett. **10**, 1012–1014 (1998).
24. A. Malcoci, A. Stöhr, K. Lill, F. Siebe, P. Van der Waal, A. Sauerwald, R. Güsten, and D. Jäger, "Optical submillimeter-wave generation employing antenna integrated ultra-fast travelling-wave 1.55µm photodetectors," in *IEEE MTT-S International Microwave Symposium Digest* (2003), Vol. 1, pp. 143–146.
25. D. B. Rutledge, D. P. Neikirk, and D. P. Kasilingam, "Integrated circuits antennas," in *Infrared and Millimeter Waves, Vol.10*, K. J. Button, ed. (Academic Press, 1983), pp. 1–90.

26. E. A. Michael, "Travelling-wave photonic mixers for increased continuous-wave power beyond 1 THz," Semicond. Sci. Technol. **20**, 164–177 (2005).
27. A. Nahata, A. S. Weling, and T. F. Heinz, "A wideband coherent terahertz spectroscopy system using optical rectification and electro-optic sampling," Appl. Phys. Lett. **69**, 2321 (1996).
28. E. Peytavit, "Highly distributed photoconductor for CW THz generation," in *2016 41st International Conference on Infrared, Millimeter, and Terahertz Waves (IRMMW-THz)* (IEEE, 2016), pp. 1–2.
29. D. R. Grischkowsky, "Optoelectronic characterization of transmission lines and waveguides by terahertz time-domain spectroscopy," IEEE J. Sel. Top. Quantum Electron. **6**, 1122–1135 (2000).
30. H. Cheng, J. F. Whitaker, T. M. Weller, and L. P. B. Katehi, "Terahertz-bandwidth pulse propagation on a coplanar stripline fabricated on a thin membrane," IEEE Microw. Guid. Wave Lett. **4**, 89–91 (1994).
31. A. W. Jackson, J. P. Ibbetson, A. C. Gossard, and U. K. Mishra, "Reduced thermal conductivity in low-temperature-grown GaAs," Appl. Phys. Lett. **74**, 2325 (1999).
32. E. Peytavit, C. Coinon, and J.-F. Lampin, "A metal-metal Fabry–Pérot cavity photoconductor for efficient GaAs terahertz photomixers," J. Appl. Phys. **109**, 016101 (2011).
33. E. Rosencher and B. Vinter, *Optoelectronics* (Cambridge University Press, 2002).
34. E. Peytavit, M. Billet, Y. Desmet, G. Ducournau, D. Yarekha, and J.-F. Lampin, "Nitrogen-ion-implanted GaAs Fabry-Pérot cavity photoconductor for THz photonics," in *IRMMW-THz 2015 - 40th International Conference on Infrared, Millimeter, and Terahertz Waves* (2015).
35. E. Y. Wu and B. H. Yu, "High-field electron transport in compensated GaAs," Appl. Phys. Lett. **58**, 1503–1505 (1991).
36. M. B. Kuppam, J.-F. Lampin, E. Peytavit, J.-F. Roux, and J.-L. Coutaz, "Study of Ultrafast Semiconductor Photoswitches for CW RF Signal Sampling and Modulation," J. Light. Technol. **32**, 3839–3845 (2014).
37. L. B. Soldano and E. C. M. Pennings, "Optical Multi-Mode Interference Devices Based on Self-Imaging: Principles and Applications," J. Light. Technol. **13**, 615–627 (1995).
38. S. Romero-García, F. Merget, F. Zhong, H. Finkelstein, and J. Witzens, "Silicon nitride CMOS-compatible platform for integrated photonics applications at visible wavelengths," Opt. Express **21**, 14036 (2013).
39. C. R. Doerr, L. Chen, Y.-K. Chen, and L. L. Buhl, "Wide Bandwidth Silicon Nitride Grating Coupler," IEEE Photonics Technol. Lett. **22**, 1461–1463 (2010).
40. A. Gorin, A. Jaouad, E. Grondin, V. Aimez, and P. Charette, "Fabrication of silicon nitride waveguides for visible-light using PECVD: a study of the effect of plasma frequency on optical properties," Opt. Express **16**, 13509 (2008).
41. F. Bavedila, V. Magnin, J. Harari, D. Yarekha, D. Troadec, S. Lepilliet, V. Avramovic, G. Ducournau, J.-F. Lampin, and E. Peytavit, "Development of an highly distributed photoconductor for CW THz generation," in *2018 43rd International Conference on Infrared, Millimeter, and Terahertz Waves (IRMMW-THz)* (IEEE, 2018), pp. 1–2.
42. D. Decoster, G. H. Jin, H. Deng, J. P. Vilcot, and J. Harari, "Investigation of 3-D Semivectorial Finite-Difference Beam Propagation Method for Bent Waveguides," J. Light. Technol. Vol. 16, Issue 5, pp. 915- **16**, 915- (1998).
43. E. Peytavit, S. Arscott, D. Lippens, G. Mouret, S. Matton, P. Masselin, R. Bocquet, J. F. Lampin, L. Desplanque, and F. Mollot, "Terahertz frequency difference from vertically integrated low-temperature-grown GaAs photodetector," Appl. Phys. Lett. **81**, 1174 (2002).
44. F. Laermer and A. Urban, "Challenges, developments and applications of silicon deep reactive ion etching," in *Microelectronic Engineering* (Elsevier, 2003), Vol. 67–68, pp. 349–355.
45. D. Van Thourhout, G. Roelkens, I. Christiaens, K. De Mesel, and R. Baets, "Thin-Film Devices Fabricated With Benzocyclobutene Adhesive Wafer Bonding," J. Light. Technol. Vol. 23, Issue 2, pp. 517- **23**, 517- (2005).
46. G. F. Engen and C. A. Hoer, "Thru-Reflect-Line: An Improved Technique for Calibrating the Dual Six-Port Automatic Network Analyzer," IEEE Trans. Microw. Theory Tech. **27**, 987–993 (1979).
47. W. Heinrich, "Quasi-TEM description of MMIC coplanar lines including conductor-loss effects," IEEE Trans. Microw. Theory Tech. **41**, 45–52 (1993).
48. C. Tannoury, M. Billet, C. Coinon, J. F. Lampin, and E. Peytavit, "Low-temperature-grown gallium arsenide photoconductors with subpicosecond carrier lifetime and photoresponse reaching 25 mA/W under 1550 nm CW excitation," Electron. Lett. **56**, 897–899 (2020).